Available online at www.sciencedirect.com
SCIENCE DIRECT®

Journal of the European Ceramic Society 24 (2004) 861–870

www.elsevier.com/locate/jeurceramsoc

Erosion and strength degradation of biomorphic SiC

A.R. de Arellano-López[a,*], J. Martínez-Fernández[a], F.M. Varela-Feria[a], T.S. Orlova[b], K.C. Goretta[c], F. Gutierrez-Mora[c], Nan Chen[c], J.L. Routbort[c]

[a]*Departamento de Física de la Materia Condensada, Universidad de Sevilla, PO Box 1065, E-41080 Seville, Spain*
[b]*Ioffe Physical-Technical Institute of the Russian Academy of Sciences, St. Petersburg 194021, Russia*
[c]*Energy Technology Division, Argonne National Laboratory, Argonne, IL 60439-4838, USA*

Received 11 January 2003; received in revised form 24 April 2003; accepted 27 April 2003

Abstract

Solid-particle-erosion studies were conducted on biomorphic SiC based on eucalyptus and pine, reaction-bonded (RB) SiC, and hot-pressed (HP) SiC. The erodents were angular SiC abrasives of average diameter 63, 143, or 390 μm and the impact velocity was 100 m s^{-1}. Impact occurred at normal incidence. Material loss in all targets occurred by brittle fracture. The biomorphic specimens eroded by formation of both lateral and radial cracks and their erosion rates were higher than both conventional SiCs. The RB SiC eroded as a classic brittle material, by formation and propagation of lateral cracks. The HP SiC, the hardest target, was the most erosion resistant. In erosion of the HP SiC, the abrasive particles, especially the largest ones, fragmented upon impact. The resulting dissipation of energy led to relatively low erosion rates. Flexural strength before and after erosion was measured for the biomorphic eucalyptus, RB SiC, and HP SiC. Erosion damage reduced the flexural strengths of all of the specimens. The relative strength reductions were lowest for the biomorphic eucalyptus and highest for the HP SiC. The hot-pressed SiC responded as predicted by accepted models of impact damage in brittle solids. The responses of the biomorphic and reaction-bonded SiC specimens were modeled as if they consisted of only SiC and porosity. This approximation agreed reasonably well with observed degradations of strength.

Keywords: Biomorphic materials; Erosion; Microstructure; Porosity; SiC; Strength; Wood

1. Introduction

A common feature in strong, lightweight materials is microstructural complexity.[1] This complexity is evidenced in biological structural materials such as wood, shells, and bones.[2] Several efforts have focused on producing artificial ceramic microstructures that resemble those of natural materials (continuous-fiber reinforced ceramics,[3] porous ceramics,[2] ceramic fibrous monoliths,[4,5] etc). Natural materials, perfected by evolution, offer optimal mechanical response with low density. Their microstructures typically contain interconnected pores.[6,7]

In recent years, a novel processing method of ceramic fabrication uses carbonized-wood templates to produce SiC by reactive gas- or liquid-Si infiltration.[8–15] The general approach consists of a rapid and controlled mineralization of the wood. The final SiC material keeps the wood microstructure and some of its excellent properties.

The mechanical properties of monolithic SiC ceramics have been studied widely.[16] Those of biomorphic SiC are less well known.[10,12–15] Among the properties of interest is resistance to solid-particle erosion,[17,18] because material loss by erosion may be a concern in certain applications, such as heat exchangers. The effects of surface damage on strength are also of concern.[19]

In this study, we have conducted solid-particle erosion tests on reaction-bonded (RB) SiC, hot-pressed (HP) SiC, and two candidate biomorphic SiCs, fabricated by liquid Si infiltration of pyrolized scaffolds of eucalyptus and pine. Strengths in flexure have also been measured before and after erosion testing. The goals of this work were to establish the response of biomorphic SiC to erosion and to determine the effects of erosive

* Corresponding author. Tel.: +34-95-455289; fax: +34-95-4612097.
E-mail address: aral@us.es (A.R. de Arellano-López).

0955-2219/03/$ - see front matter © 2003 Elsevier Ltd. All rights reserved.
doi:10.1016/S0955-2219(03)00321-2

damage on strength in comparison to the responses of conventional SiC ceramics.

2. Experimental procedures

2.1. Specimen preparation and microstructure

Basic features of biomorphic SiC fabrication process have been described elsewhere.[10–15] The first step was selection of appropriate wood precursors to achieve a particular microstructure and set of properties.[15] Each wood was cut to a basic shape, and then pyrolized in Ar at 1000 °C. The resulting carbon templates lost ≈60% of the initial weight and about 70% of the initial volume, but kept intact the microstructure of the wood.[13] The templates were shaped carefully and infiltrated in vacuum with molten Si at 1550 °C. SiC formed by a rapid and spontaneous reaction, without measurable change of volume or shape of the template.

Sufficient reaction and good mechanical properties can be achieved with pore sizes >5 μm. To produce good final products, excess Si over the stoichiometric amount is always necessary (20–100%), with the excess increasing as the typical pore size of the template increases. If necessary, unreacted Si can be removed from the material in a second heating cycle in which Si is soaked away from the porous structure by a carbon cloth. Final biomorphic SiC materials are always a combination of SiC with some unreacted Si and C.[20]

For this study, Flanders pine and white eucalyptus were selected. The first had a typical density of 0.53 g cm^{-3} and the second 0.84 g cm^{-3}. They represented lower and higher ranges of densities and microstructures for efficient infiltration. Final products were, respectively, 1.7 ± 0.1 and 2.0 ± 0.1 g cm^{-3}. The initial excess of Si was larger in the pine than in the eucalyptus. The first had maximum SiC fraction of 34% and the second 63% when the reaction was complete.

The microstructures of carbon templates of the SiC materials are documented in Figs. 1 and 2. The intrinsic anisotropy of the wood was transferred to the biomorphic SiC. [Along the length of the tree (axial), the materials are typically stronger than in the perpendicular direction (radial).[14]] The pore structures of the two types of wood were vastly different. Pine exhibited basically a single-modal porosity that covered ≈50% of the section, as measured in the carbon perform, with a typical size of 15 μm. Dispersion of porosity size was due to differences in the wood cell size in different seasons. Eucalyptus exhibited bimodal porosity. Large pores from the vascular vessels of the tree, with an average size of 21 μm, covered 12% of the section, as measured in the carbon template. Small pores from the wood cells, with a typical size of 2.1 μm, covered 30% of the section.[15]

The RB SiC was archival material from earlier erosion tests, Noralide NC-430 (Norton, Worcester, MA, USA). It consisted of 88.5 wt.% SiC and 10.5 wt.% Si in a duplex microstructure. The RB SiC consists of 50 vol.% large (≈100 μm) SiC grains, surrounded by a two-phase mixture consisting of 35 vol.% small SiC grains and 15 vol.% Si. Details can be found in the literature.[17,18] The HP SiC was also tested previously: NC-203 (Norton, Worcester, MA, USA) consisted of

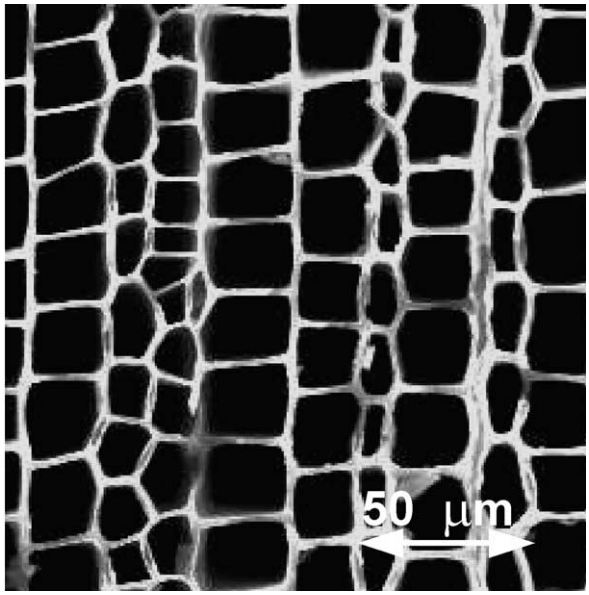

Fig. 1. Microstructure of the carbon template of a Flanders pine perform, that keeps the same microstructure of the starting wood. A single-mode array of cells is evident in this radial cross section.

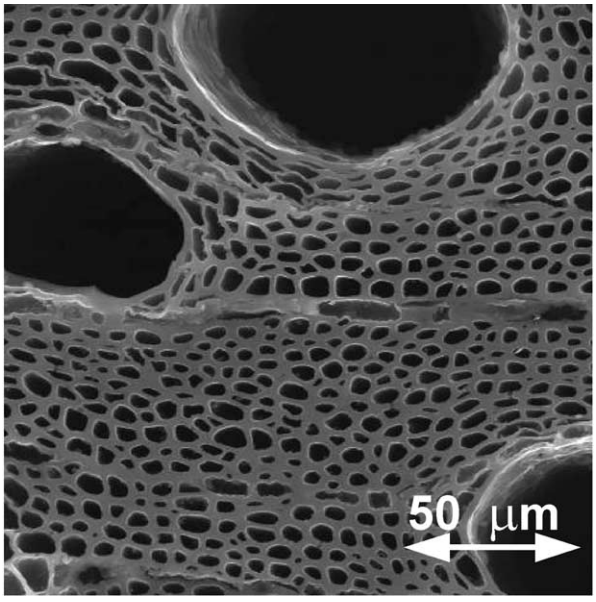

Fig. 2. Microstructure of the carbon template of a white eucalyptus perform, that keeps the same microstructure of the starting wood. A bi-modal array of cells is evident in this radial cross section.

95–99% SiC having an average grain size of ≈2–3 μm, with a maximum grain size of ≈10 μm. Both materials were >99% dense.[18,21]

Specimens for erosion testing were cut from billets with a diamond-bladed saw. The average specimens for determination of erosion rate were approximately 3×10××25 mm for the eucalyptus-based SiC, 3×20×25 mm for the pine-based SiC, and 3×25×25 mm for the RB and HP SiC. No surfaces were polished. Smaller specimens were also prepared for study of individual impact sites.[22,23] These were polished with 1-μm diamond paste.

Specimens for fracture tests were prepared from eroded and as-received materials. For the eroded materials, fracture specimens were cut to widths of approximately 3 mm. Final specimen dimensions were approximately 3×3×25 mm. No surfaces were polished because of the relatively porous structures of the biomorphic ceramics. Polishing would not be likely to alter flaw population significantly. Similar specimens were cut from as-received materials. The tensile surfaces of the RB and HP SiC specimens were polished with 1-μm diamond paste and the edges were beveled.

2.2. Erosion and strength tests

Solid-particle erosion tests were carried out in a slinger-type apparatus that has been described previously.[24] Tests were conducted in vacuum (approx. 500 mTorr), and thus aerodynamic effects were negligible. The feed rate of the erodent was ≈8 g/min. At such a slow rate, interactions between particles were negligible.

The erodent particles were angular SiC abrasives (Norton Co., Worcester, MA, USA) with mean diameter (D) of 63, 143, or 390 μm.[24] The particle velocity was 100 m s^{-1} and the angle of impact was 90°. Two specimens of each type of SiC were eroded under each set of conditions. The eroded surfaces of the biomorphic SiC specimens were ≈8–20×19 mm; the eroded surfaces of the RB and HP SiC specimens were 19×25 mm. Steady-state erosion rates (ER, in mg g^{-1}) were determined from plots of the specimen weight loss versus weight of particles impacting the surface. At least four runs were conducted for each specimen. Following each run, specimens were removed, brushed, cleaned by an air blast, and weighed. It is estimated that the average weight-loss measurements were accurate to ±2%. The uncertainty arose due to slightly incomplete cleaning of the surfaces.

Specimens eroded with 143-μm SiC were used for post-erosion strength tests. Four-point fracture tests were conducted with an Instron Model 4505 apparatus (Canton, MA, USA). The loading rate was 0.5 mm min^{-1}. The inner load span was 6 mm and the outer load span was 19 mm. The maximum size of the erosion specimens determined the size of the samples used for strength testing. The relatively small sample size could affect strength results.

Eroded and fractured surfaces were examined by scanning electron microscopy (SEM). Single-impact damage sites were also examined by SEM in order to elucidate the weight-loss mechanism. All specimens were coated with Au–Pd and examined in a JEOL 5400 (Peabody, MA) or Hitachi S-4700-II microscope (Tokyo, Japan).

3. Results

3.1. Erosion tests

Representative data for weight loss versus dose of impacting SiC particles are shown in Fig. 3. ER values were defined as the slopes of linear least-squares fits to the data. The results for the HP SiC were consistent and nearly identical. The RB SiC, which exhibited some microstructural variation, also exhibited slight scatter in the data. The biomorphic SiC specimens exhibited significant apparent variation in the weight-loss data. This variation is attributable to differences in eroded areas between nominally identical specimens, and to differences in erosion rate caused by microstructural effects.

Data of erosion rate versus average diameter of impacting particles are shown in Fig. 4. In two commonly cited models of erosion of brittle materials, the quasistatic model of Wiederhorn and colleagues[25,26] and the dynamic model of Evans et al.,[27] it is predicted that $ER \propto \propto D^{0.7}$. Power-law fits to the data of Fig. 4 are shown in Table 1. The RB SiC and pine-based biomorphic SiC data fit the prediction of the models reasonably well, the eucalyptus-based biomorphic SiC less

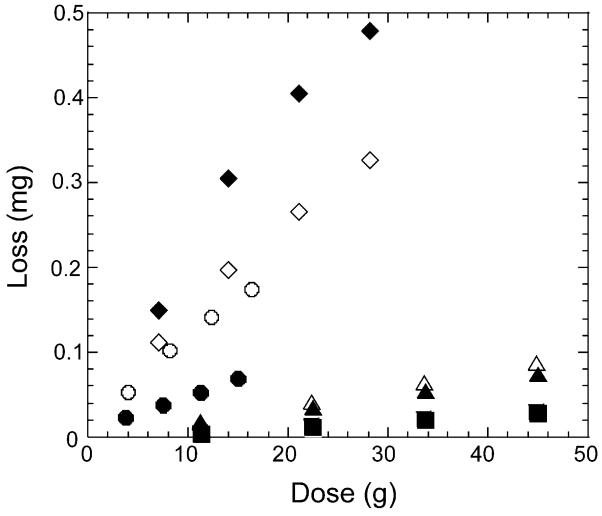

Fig. 3. Weight loss vs. erodent dose for specimens eroded by 143-μm SiC at 100 m/s: biomorphic eucalyptus (circles), biomorphic pine (diamonds), RB SiC (triangles), and HP SiC (squares—the open squares are covered by filled squares).

well, and the HP SiC not at all. In fact, the particle-diameter exponent was negative for the HP SiC.

The first question related to microstructure is the condition of the erodent after testing. Most useful models of erosion response are based on the erodent particles remaining intact.[25–31] None of the particles exhibited significant fracturing when striking the RB SiC or biomorphic targets. When striking the HP SiC, the 63-μm SiC exhibited virtually no and the 143-μm SiC minor fracturing. However, the 390-μm SiC exhibited substantial fracturing (Fig. 5).

The single-impact sites were generally characteristic of erosion of brittle solids. Little difference was observed among the various types of SiC. Three basic types of events were observed. Some of the impacts evinced all of the features that lead to material removal: indenting, radial-crack formation, and spalling of the target caused by propagation of lateral cracks (Fig. 6). Most impact sites were similar, but crack development was not so clear (Fig. 7). Fracture patterns at damage sites in the

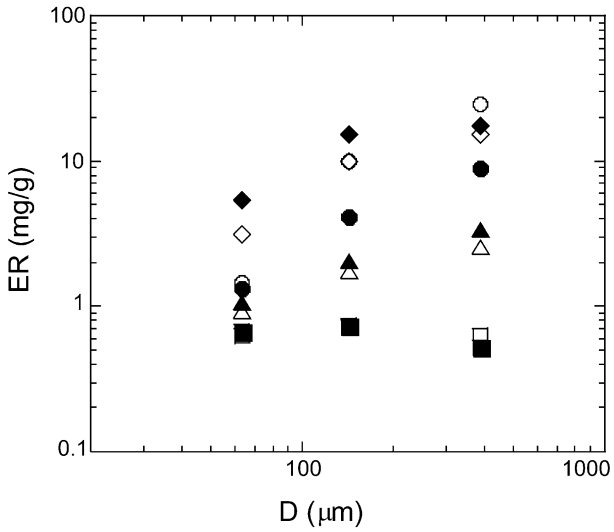

Fig. 4. ER vs. SiC erodent diameter D for biomorphic eucalyptus (circles), biomorphic pine (diamonds), RB SiC (triangles), and HP SiC (squares).

Table 1
Erodent mean-diameter exponent and linear correlation coefficient R for erosion of various SiC ceramics by angular SiC particles

Specimen	D exponent	R value
Eucalyptus 1	1.53	0.977
Eucalyptus 2	1.04	0.990
Pine 1	0.85	0.940
Pine 2	0.63	0.843
Hot-pressed 1	−0.003	0.032
Hot-pressed 2	−0.14	0.685
RB 1	0.55	0.983
RB 2	0.62	0.992

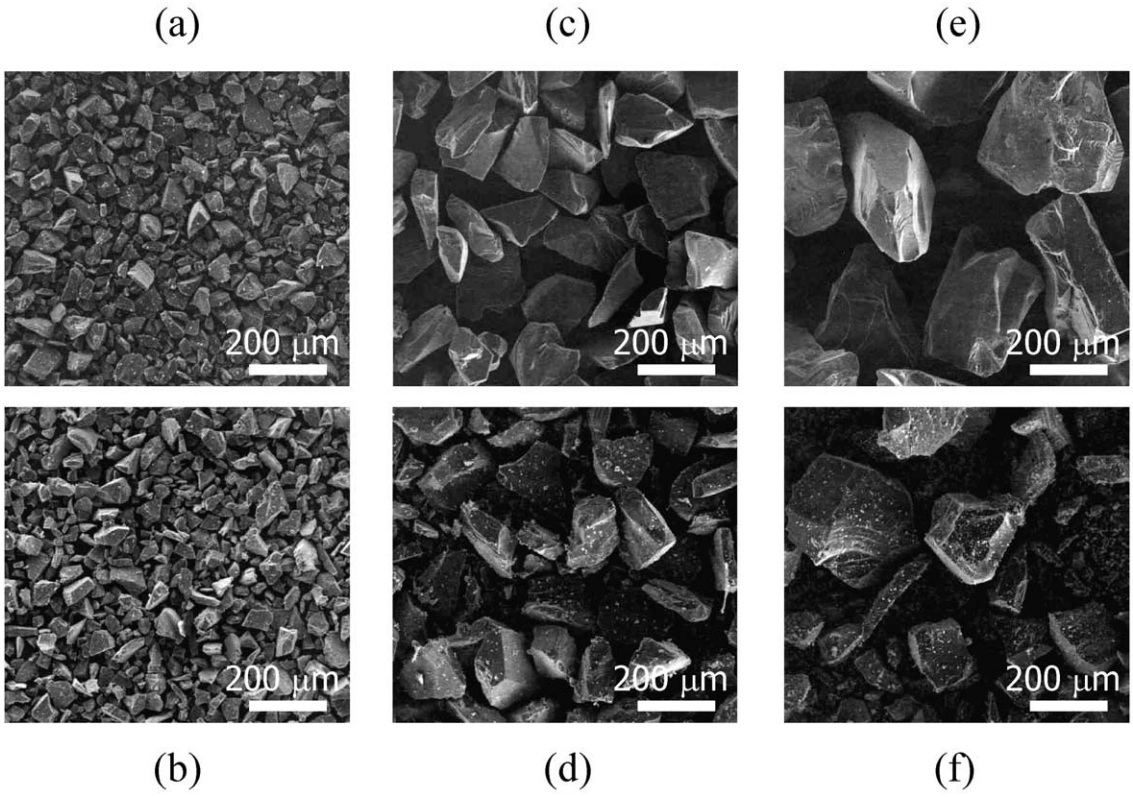

Fig. 5. SEM photomicrographs of SiC erodent particles that struck the HP SiC: 63-μm SiC (a) before and (b) after impact; 143-μm SiC (c) before and (d) after impact; and 390-μm SiC (e) before and (f) after impact.

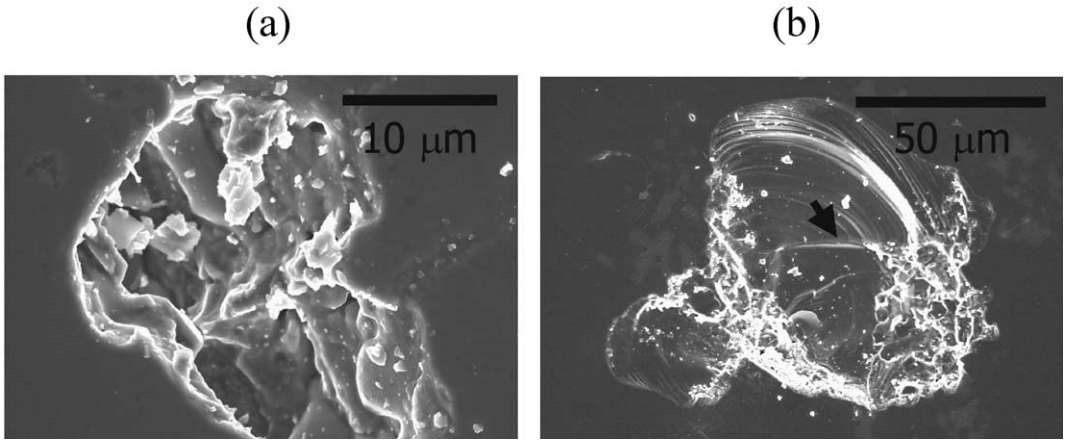

Fig. 6. SEM photomicrographs of single impact by 143-μm SiC erodent: (a) biomorphic pine and (b) RB SiC. Radial crack indicated by arrow.

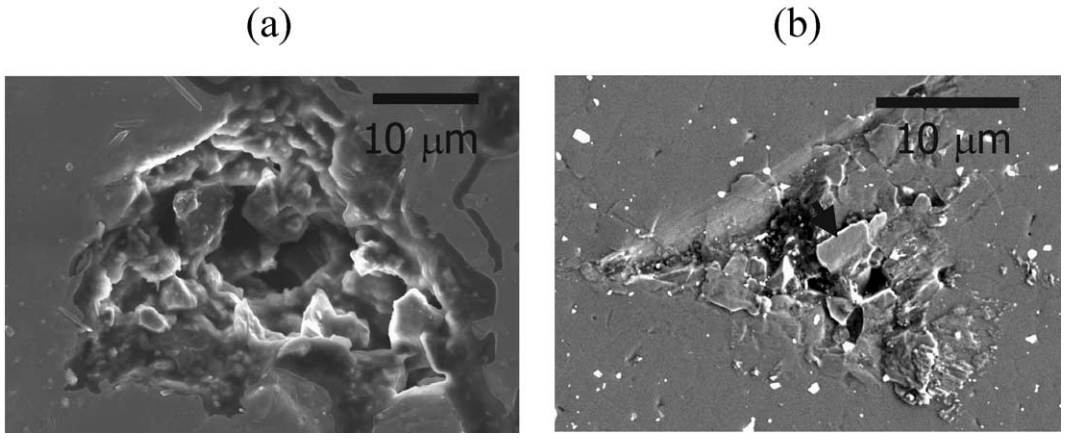

Fig. 7. SEM photomicrographs of single impact by 143-μm SiC erodent: (a) biomorphic pine, in which a variable microstructure is evident; (b) HP SiC, in which damage and plasticity are evident.

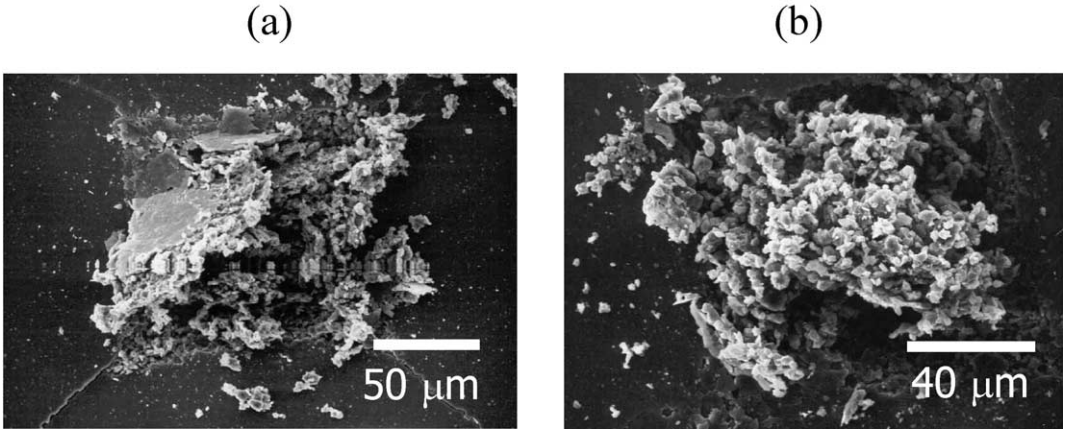

Fig. 8. SEM photomicrographs of single impact of HP SIC by 390-μm SiC erodent: (a) classical radial and small lateral cracks, and fracture debris from the erodent, are evident; (b) significant fracture and embedding of erodent are observed.

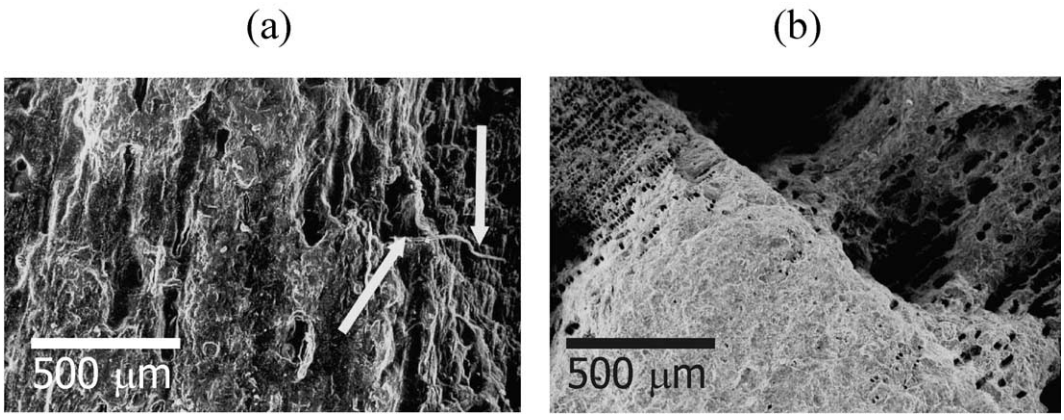

Fig. 9. SEM photomicrograph of steady-state surfaces of (a) biomorphic eucalyptus, for which voids are evident and relatively large sections appear to have been removed (arrows); (b) biomorphic pine, in which large voids and finer channels are evident.

Table 2
Four-point flexural strength before (σ_o) and after (σ_{er}) erosion testing

Specimen	σ_o (MPa)	σ_{er} (MPa)	% decrease
Eucalyptus	130±12	98±36	25
Pine	Not tested	Not tested	–
Hot-pressed	570±28	267±140	53
RB	245±20	168±30	31

eroded biomorphic SiC specimens revealed the complex microstructures of these ceramics, which consists primarily of a strongly interconnected SiC frame and unreacted Si and C.

As expected, the size of the damage site scaled with D. However, impact by the HP SiC by 390-μm SiC yielded damage sites with different appearances. In particular, clear evidence of significant fracturing of the SiC erodent was observed (Fig. 8).

The steady-state erosion surfaces all indicated similar mechanisms of material removal. Brittle, cleavage-like fracture was dominant. At high magnification, all types of SiC exhibited similar eroded surfaces. At lower magnification, the biomorphic SiC exhibited several relatively large holes and smaller channels indicative of the fibrous structure of the host woods (Fig. 9). Many of the pine- and one of the eucalyptus-based SiC specimens fractured during erosion testing when they were clamped into their holder.

3.2. Strength tests

Results of the four-point flexural tests are shown in Table 2. The pine-based SiC was not tested because it was too porous to remain intact throughout the erosion testing. The scatter in the strength data reflects both statistical standard deviation and estimates of measurement accuracies. From two to four specimens were tested per condition.

As expected, the HP SiC was initially the strongest and the eucalyptus-based SiC the weakest. The average strengths of 570 MPa for the HP SiC and 245 MPa for the RB SiC were typical of what is commonly obtained.[32] The lower strength of the eucalyptus-based SiC is attributable to its porous microstructure.[12,14]

Erosive damage was least severe in the HP SiC, but its effect on strength was the greatest. The reduction of strength in the RB SiC is also evident after erosion. On the other hand, less significant reduction of strength was measured in the eucalyptus-based SiC. Even though the average strength decreased, the error bars of the strength measurements, 130±12 MPa before erosion and 98±36 MPa after erosion, overlapped.

SEM examination of fracture surfaces revealed that cleavage dominated the fracture processes. The RB SiC exhibited two scales of fracture events. Large cleavage fractures were evident in the SiC regions, and finer cleavage fractures were evident in the duplex SiC+Si regions between the larger SiC aggregates. In places, the HP SiC exhibited a mixture of transgranular cleavage and intergranular fracture (Fig. 10).

4. Discussion

4.1. Erosion results

Erosive damage from sharp particles impacting dense brittle solids has been studied for decades and models are effective in predicting a material's response. With impact at normal or near-normal incidence, material loss occurs from the following sequence of events: (1) Indentation creates an elastic-plastic zone beneath the impacting particle. (2) Radial cracks perpendicular to the specimen surface are created beneath the elastic-plastic zone. (3) As the erodent particle recoils, a resulting tensile stress state induces formation of lateral cracks approximately parallel to the surface. (4) The lateral cracks propagate to the surface and chips are removed.[25,27] The models are based on energy transfer to the target. Given that the scale of the damage was

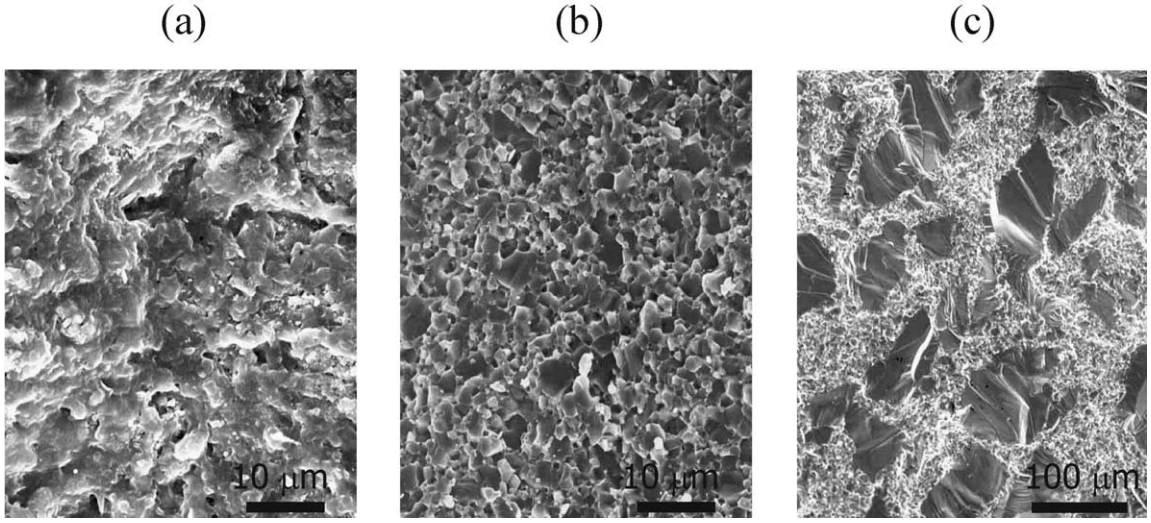

Fig. 10. SEM photomicrographs fracture surface of: (a) biomorphic eucalyptus, in which cleavage predominates; (b) HP SiC, in which some intergranular fracture is evident; and (c) RB SiC, which exhibits two scales of cleavage.

small relative to the biomorphic SiC membrane thickness, these models should apply. If the erodent particles fracture significantly, the models may lose some of their utility.[28,30]

Taking the dynamic models of Evans and coworkers as representative, for impact pressure p, radial cracks of length c_R form:

$$c_{\mathrm{R}} = \left[F^{*}(E/\mathrm{H})^{1/2}/K_{\mathrm{c}}H^{1/4}\right]^{2/3}p^{2/3}, \tag{1}$$

where F^{*} is a geometric factor, E is the target elastic modulus, K_{c} is the target toughness, and H is the target hardness.[31,33] The lateral cracks that form have length c_{L}

$$c_{\mathrm{L}} = A\left[F(E/H)^{3/4}/K_{\mathrm{c}}H^{1/4}\right]^{1/2}p^{5/8}, \tag{2}$$

where A is a constant, F is a geometric factor, and the other terms are as defined in Eq. (1). Longer cracks imply more rapid erosion,[34] with the volume of material removed varying as approximately c_L^2. In conventional monolithic ceramics, when particles impact at near-normal incidence, lateral cracks induce mass loss, but the radial cracks do not contribute significantly to material removal.[25–31,33–35] For impact at oblique incidence, however, radial cracks can lead to material removal.[36]

Erosion rates expressed in terms of volume (ER_{v}) can be predicted from particle impact parameters and target materials properties. Taking, as an example, the model of Wiederhorn and coworkers for erosion of brittle solids by sharp particles,[25,26,37]

$$ER_v \propto V^{2.4}R^{3.7}\rho^{1.2}K_c^{-1.3}H^{0.11}, \tag{3}$$

where V is the particle velocity, R is the particle radius, ρ is the particle density, and K_{c} and H are as defined previously. If erosion rate is expressed on a mass basis, then for radius R (or, equivalently, diameter D)

$$ER \propto R^{0.7} \tag{4}$$

The prediction of $ER \propto D^{0.7}$ was approximately valid for the pine-based SiC and the RB SiC, but not for the eucalyptus-based SiC or the HP SiC (Table 2). The data sets shown in Figs. 3 and 4 were sufficiently consistent that deviations from the predicted dependence of ER on D can be interrogated. The eucalyptus exhibited a stronger dependence on D than predicted. The most likely cause derives from its microstructure, which replicated that of the host wood. Channels and pores were present (Figs. 1 and 2), and they affected erosion significantly.

It has been shown, for example, that for impact of brittle materials at oblique incidence, the radial cracks that are produced are at an angle to the surface and that they can contribute to material loss from the target.[36] Radial cracks can also contribute to material loss when they drive through a relatively thin wall. Such an event is shown schematically in Fig. 11. The shaded region is lost without formation of lateral cracks. Larger erodents produce deeper radial cracks. The propensity for material loss to occur from radial cracking should increase with erodent diameter. If such a mechanism represents a significant fraction of the total wastage, then a stronger-than-predicted dependence of ER on D should result, as occurred for the eucalyptus.

This speculation is supported by three additional pieces of information. The pine also featured pores and channels, but the SiC walls of the pine were thicker than those of the eucalyptus. The average D exponent for the pine was 0.74, which is slightly greater than predicted for material loss by purely lateral-crack formation. Thus, the pine data follow, at least approximately, the

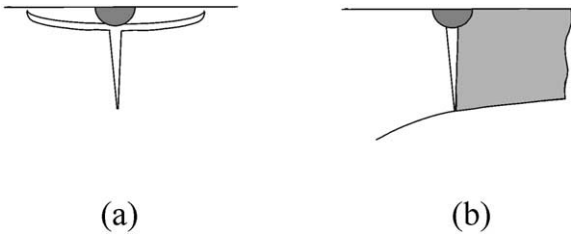

Fig. 11. Schematic diagram of erosive damage in SiC ceramics: (a) conventional mechanism of indentation producing an elastic-plastic zone and radial crack, followed by lateral crack formation as the erodent particle recoils; (b) impact into thin member in which radial crack induces material loss.

expected trend implied by consideration of radial cracks. More importantly, SEM images of the eroded surfaces of the eucalyptus exhibit clear evidence of relatively large-scale material removal (Fig. 9a). These larger-scale events may be related to wall fractures caused by radial cracks. Most importantly, the erosion rates of the biomorphic SiC specimens were all significantly higher than for the monolithic SiC specimens. Material loss by combined action of lateral and radial cracks could account for the differences.

On the other end of the spectrum, the HP SiC exhibited a much weaker dependence of *ER* on *D* than predicted. The data in Fig. 2 can be divided into two response regimes. There were slight increases in erosion rate with an increase in *D* from 63 to 143 μm. There were then clear decreases in *ER* with an increase in *D* from 143 to 390 μm. As shown in Fig. 5, the 63-μm did not fracture upon impact into the HP SiC, the 143-μm erodent fractured only somewhat, and the 390-μm erodent fractured into small pieces. Larger erodents contain more severe flaw populations and are subject to more severe shock during impact. They are thus much more susceptible to fracturing during impact than are smaller particles. This size-dependent response has been observed previously; it is especially severe when the target is as hard or harder than the erodent.[18,29–31] Of the four targets in this study, only the HP SiC was as hard as the erodent.

When an erodent particle fractures, some of the kinetic energy of the impact is converted into surface energy. Less energy is imparted to the target, and thus erosive processes remove less material. A reduced dependence of *ER* on *D* results. If the fracturing is severe, as was the case for the SiC erodent, a negative dependence of ER on D can result.

Although the erosion data exhibited target-dependent relations between *ER* and *D*, the basic material-removal mechanisms by brittle fracture were similar. The fraction of material loss caused by radial or lateral cracks varied among the biomorphic and the RB and HP SiC, and the loss was least in the HP SiC because of its hardness. The basic fracture mechanism was, however, brittle cleavage in all cases. And, for all of the target materials, erosion induced significant surface damage.

4.2. Strength results

Strength degradation caused by erosion of the various SiC specimens can be separated into two materials considerations. The HP SiC is considered to be an ideal dense ceramic, while the RB SiC and eucalyptus-based SiC, can be considered in this analysis to be effectively a porous SiC ceramics. Metallic Si filling the porosity is not expected to play an important role in flexure strength.

Radial cracks are responsible for strength degradation.[35,38] SEM observations indicated that radial cracks did indeed form in the various SiC specimens. Fracture strength σ_f can be related to flaw length c_f by

$$\sigma_f = A \quad Z \quad K_c/\left(Y \quad c_f^{1/2}\right) \tag{5}$$

where A is a constant equal to 0.47 for a theoretical indentation radial crack, Z is a flaw-shape parameter (equal to $\pi/2$ for a semicircular flaw), and Y is a numerical constant that depends on loading and flaw size. The value of A can increase if residual stresses are relieved by the flaw.[35,38]

Taking values in Eq. (5) from the analysis of Ritter et al.,[35] $A = 0.82$, $Z = \pi/2$, and $Y = 1.9$, an estimate can be made of the critical flaw size after erosion for the HP SiC. K_c was estimated[32] as being 3.5 Mpa $m^{1/2}$. A value of 8 μm was calculated for c_R, which is reasonable when compared with the average crater size, for which $c_R \sim c_L = 0.5D$ (Fig. 7).

Strength degradation in the HP SiC appeared to follow closely expectation from models for erosion of brittle solids. Understanding of strength response of biomorphic SiC, in comparison to denser SiC, can be achieved through a framework developed for porous solids.[2,39] Previous work on the crushing strength of biomorphic SiC has shown that eucalyptus-based SiC possesses a well-connected and resistant structure.[12,14] With respect to fracture properties, the materials of this study can be regarded as (1) a fully dense structure–HP SiC, (2) an 15%-porous structure–RB SiC, and (3) a 37%-porous structure–eucalyptus, because the influence of the Si can be neglected. For such a range of porosity, a successful theory of solids, due to Rice, is based on the concept that minimum solid area controls physical properties.[39] Minimum solid area not only depends on the fraction of porosity, but also on its type, geometry, and distribution. The operant equation is:

$$\frac{\sigma}{\sigma_{FD}} = e^{-f(P)} \tag{6}$$

where σ is the strength of the porous body, σ_{FD} is the strength of the fully dense body, $f(P)$ is a polynomial

function of the porosity fraction which forms depends on the topology of the porosity. In our study, the fully dense body is considered to be the HP SiC.

In Fig. 12, we have plotted the logarithm of the strengths σ of the RB SiC and biomorphic eucalyptus, normalized by the strength of the HP SiC (σ_{HP}), vs. porosity fraction (P) for the two sets of data: uneroded and eroded. The relative strengths of the uneroded porous ceramics are lower than those of the eroded ceramics. We speculate that the reason for this is that flexural strength is dominated by imperfections. A polished surface of fully dense SiC is significantly more perfect than polished surface of RB and biomorphic SiC. In contrast, all of the eroded surfaces contain similar populations of imperfections induced by impact damage, and so a systematic underestimation of the σ/σ_{HP} relationship is possible for the uneroded porous specimens.

Phenomenologically-based predictions of Rice theory[39] for different pore morphology and distribution have been also plotted in Fig. 12. For RB SiC, spherical pores (Sph Pores Cubic) and close-packed spherical particles (Sph Part Rhom) have been considered. For biomorphic eucalyptus-based SiC, cylindrical pores, perpendicularly oriented to the stress, have been considered. Within its plane, cylindrical pores can be aligned (Cyl Pores Align) or randomly oriented (Cyl Pores Random). Our measured strengths fall correctly within the intervals so constructed.

It is possible to argue that for both materials, microstructural features are a combination of the basic types suggested above. The microstructure of the RB SiC is probably more similar to a distribution of spherical pores, and that of biomorphic SiC is more similar to a distribution of cylindrical pores, with a significant, although not complete, degree of alignment. Given the underestimation argument given above, the concordance of our results with the minimum-solid-area theory is quite good. Similar concordance was also recently reported for high-temperature crushing strength of a variety of siliconized SiC, of the same kind used in this study.[40]

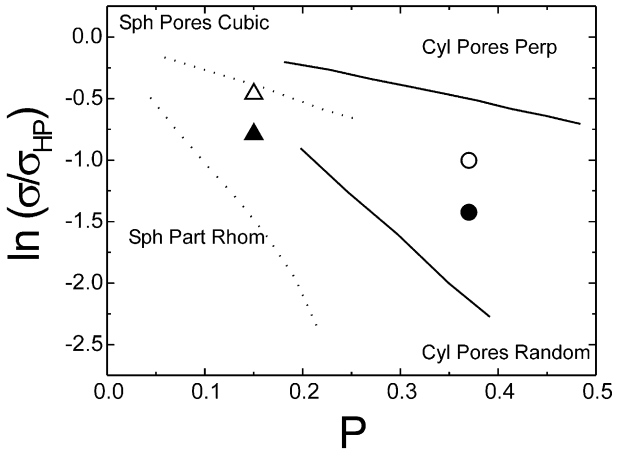

Fig. 12. Strength before denoted by filled points and after erosion denoted by open points of biomorphic eucalyptus (circles) and RB SiC (triangles), normalized by corresponding strength of fully dense HP SiC vs. fraction of porosity (defined as fraction not SiC).

5. Conclusions

Solid-particle erosion of biomorphic SiC based on eucalyptus and pine, RB SiC, and HP SiC occurred by brittle fracture. The biomorphic specimens eroded by formation of both lateral and radial cracks and their erosion rates were the highest. The RB SiC eroded as a classic brittle material, by formation and propagation of lateral cracks. The HP SiC was the hardest material and the most erosion resistant. For the HP SiC, the SiC erodents, especially the largest ones of 390 μm average size, fragmented upon impact. The resulting dissipation of impact energy led to low erosion rates.

Erosion damage induced flexural-strength degradation in all of the SiC specimens. The HP responded as predicted by models of impact damage; its relative reduction in strength was the highest. The responses of the biomorphic and RB SiC specimens were modeled as if they consisted of only SiC and porosity. This approximation agreed reasonably well with the strength data and SEM observations.

Acknowledgements

We thank T. Tran for experimental assistance. This work was supported by the Ministerio de Educación y Ciencias of Spain, under Project MAT2000-1533-C03-03, and by the Andalusian Government, under a Technology Transfer Project (2001); the Russian Academy of Sciences; and the US Department of Energy, under Contract W-31-109-Eng-38.

References

1. Wachtman, J. B., *Mechanical Properties of Ceramics*. John Wiley and Sons, New York, 1996.
2. Gibson, L. J. and Ashby, M. F., *Cellular Solids: Structure and Properties*. Pergamon Press, 1988.
3. Naslain, R., Materials design and processing of high-temperature matrix composites: state of the art and future trends. *Adv. Comp. Mater.*, 1999, **8[1]**, 3–16.
4. Kovar, D., King, B. H., Trice, R. W. and Halloran, J. W., Fibrous Monolithic Ceramics. *J. Am. Ceram. Soc.*, 1997, **80[10]**, 2471–2487.
5. de Arellano-López, A. R., López-Pombero, S., Domínguez-Rodríguez, A., Routbort, J. L., Singh, D. and Goretta, K. C., Plastic deformation of silicon nitride/boron nitride fibrous monoliths. *J. Eur. Ceram. Soc.*, 2001, **21**, 245–250.
6. Alper, M., The biological membrane. *Mater. Res. Bull.*, 1992, **17**, 53–60.

7. Mark, J. E. and Calvert, P. D., Biomimetic, hybrid and in-situ composites. *Mater. Sci. Eng.*, 1994, **C1**, 159–170.
8. Greil, P., Lifka, T. and Kaindl, A., Biomorphic silicon carbide ceramics from wood: I and II. *J. Eur. Ceram. Soc.*, 1998, **18**, 1961–1983.
9. Greil, P., Near net shape manufacturing of ceramics. *Mater. Chem. Phys.*, 1999, **61**, 64–68.
10. Martínez-Fernández, J., Varela-Feria, F. M. and Singh, M., Microstructure and thermomechanical characterization of biomorphic silicon carbide-based ceramics. *Scripta Mater.*, 2000, **43**, 813–818.
11. Singh, M., Environment conscious ceramics (Ecoceramics). *Ceram. Sci. Eng. Proc.*, 2000, **21[4]**, 39–44.
12. Varela-Feria, F. M., López Pombero, S., Martínez-Fernández, J., de Arellano-López, A. R. and Singh, M., Creep resistant biomorphic silicon-carbide based ceramics. *Ceram. Eng. Sci. Proc.*, 2001, **22[3]**, 135–145.
13. Martinez-Fernández, J., de Arellano-López, A. R., Varela Feria, F. M. and López-Pombero, S., Maderas cerámicas: fabricación y propiedades del carburo de silicio biomórfico. *Bol. Soc. Esp. Ceram. y Vidrio*, 2002, **41[4]**, 377–384.
14. Varela-Feria, F. M., Martínez-Fernández, J., de Arellano-López, A. R. and Singh, M., Low-density biomorphic silicon carbide: microstructure and mechanical properties. *J. Eur. Ceram. Soc.*, 2002, **22**, 2719–2725.
15. Varela-Feria, F. M., López-Robledo, M. J., Martínez-Fernández, J., de Arellano-López, A. R. and Singh, M., Precursor selection for property optimization in biomorphic SiC ceramics. *Ceram. Eng. Sci. Proc.*, 2002, **23[4]**, 681–685.
16. *Ceramic Source*, *Vol. 6*. Am. Ceram. Soc, Westerville, OH, 1990.
17. Routbort, J. L. and Turner, A. P. L., The erosion rate of reaction-bonded SiC containing various amounts of free silicon. *Wear*, 1983, **84**, 381–385.
18. Routbort, J. L., Scattergood, R. O. and Turner, A. P. L., The erosion of reaction-bonded SiC. *Wear*, 1980, **59**, 363–375.
19. Strzepa, P., Zamirowski, E. J., Kupperman, J. B., Goretta, K. C. and Routbort, J. L., Indentation, erosion and strength degradation of silicon-alloyed pyrolytic carbon. *J. Mater. Sci.*, 1993, **28**, 5917–5921.
20. Varela-Feria, F.M., Fabricación, microestructura y propiedades mecánicas de SiC biomórfico, M.S. Thesis, Universidad de Sevilla, 2003.
21. Routbort, J. L. and Matzke, J., On the correlation between solid-particle erosion and fracture parameters in SiC. *J. Mater. Sci.*, 1983, **18**, 1491–1496.
22. Routbort, J. L. and Scattergood, R. O., Solid-particle erosion of ceramics and ceramic composites. In *Erosion of Ceramic Materials*, ed. J. E. Ritter. Trans Tech. Publications, Geneva, Switzerland, 1992, pp. 23–51.
23. Routbort, J. L., Degradation of structural ceramics by erosion. *J. Nondestr. Eval.*, 1996, **15**, 107–112.
24. Routbort, J. L. and Scattergood, R. O., The erosion of silicon single crystals. *J. Am. Ceram. Soc.*, 1980, **63**, 635–640.
25. Wiederhorn, S. M. and Lawn, B. R., Strength degradation of glass impacted with sharp particles: I. *J. Am. Ceram. Soc.*, 1979, **62**, 66–70.
26. Ruff, A. W. and Wiederhorn, S. M., Erosion by solid particle impact. In *Treatise on Materials Science and Technology*, ed. C. M. Preece. Academic Press, New York, 1979, pp. 69–126.
27. Evans, A. G., Gulden, M. E. and Rosenblatt, M., Impact damage in brittle materials in the elastic-plastic regime. *Proc. R. Soc. London Ser. A*, 1978, **361**, 343–365.
28. Srinivasan, S. and Scattergood, R. O., Effect of erodent hardness on erosion of brittle materials. *Wear*, 1988, **128**, 139–152.
29. Routbort, J. L. and Scattergood, R. O., Anomalous solid-particle erosion rate of hot-pressed silicon carbide. *J. Am. Ceram. Soc.*, 1980, **63**, 593–595.
30. Routbort, J. L., Chu, C. Y., Roberts, J. M., Singh, J. P., Wu, W. and Goretta, K. C., Erosion of ceramic composites by various erodents. In *Proceedings Corrosion-Erosion-Wear of Materials at Elevated Temperatures*, ed. A. V. Levy. Nat. Assoc. Corr. Eng., Houston, 1991, pp. 31/3–31/9.
31. Evans, A. G., Impact damage in ceramics. In *Fracture Mechanics of Ceramics, Vol. 3*, ed. R. C. Bradt, D. P. H. Hasselman and F. F. Lange. Plenum, New York, 1978, pp. 303–331.
32. Chemical and physical properties of Si_3N_4 and SiC ceramics. In *Ceramic Source, Vol. 6*, Am. Ceram. Soc., Westerville, OH, 1990, p. 351.
33. Lawn, B. R., Evans, A. G. and Marshall, D. B., Elastic/plastic indentation damage in ceramics: the median/radial crack system. *J. Am. Ceram. Soc.*, 1980, **63**, 574–581.
34. Marshall, D. B., Lawn, B. R. and Evans, A. G., Elastic/plastic indentation damage in ceramics: the lateral crack system. *J. Am. Ceram. Soc.*, 1982, **65**, 561–566.
35. Ritter, J. E., Strzepa, P., Jakus, K., Rosenfeld, L. and Buckman, K. J., Erosion damage in glass and alumina. *J. Am. Ceram. Soc.*, 1984, **67**, 769–774.
36. Srinivasan, S. and Scattergood, R. O., On lateral cracks in glass. *J. Mater. Sci.*, 1987, **22**, 3463–3469.
37. Wiederhorn, S. M. and Hockey, B. J., Effect of material parameters on the erosion resistance of brittle materials. *J. Mater. Sci.*, 1980, **18**, 766–780.
38. Marshall, D. B., Surface damage in ceramics: implications for strength degradation, erosion and wear, ed. F. L. Riley. Nitrogen Ceramics, Nijhoff, The Hague, 1983.
39. Rice, R. W., *Porosity of Ceramics*. Marcel Dekker Inc., New York, 1998.
40. Martínez-Fernández, J., Muñoz, A., de, Arellano-López, A. R., Varela-Feria, F. M., Domínguez-Rodríguez, A. and Singh, M., Microstructure–mechanical property correlation in siliconized silicon carbide ceramics. *Acta Mater.*, 2003, **51**, 3259–3275.